SCIENTIFIC REPORTS

OPEN

A comparative analysis of secreted protein disulfide isomerases from the tropical co-endemic parasites *Schistosoma mansoni* and *Leishmania major*

Received: 6 March 2019
Accepted: 10 June 2019
Published online: 02 July 2019

Adriana E. Miele[1,2], Sofiane Badaoui[2], Lorenzo Maugliani[1,2], Romain Salza[2], Giovanna Boumis[1], Silvia Chichiarelli[1], Bertrand Duclos[2] & Sylvie Ricard-Blum[2]

The human parasites *Schistosoma mansoni* and *Leishmania major* are co-endemic and a major threat to human health. Though displaying different tissue tropisms, they excrete/secrete similar subsets of intracellular proteins that, interacting with the host extracellular matrix (ECM), help the parasites invading the host. We selected one of the most abundant proteins found in the secretomes of both parasites, protein disulfide isomerase (PDI), and performed a comparative screening with surface plasmon resonance imaging (SPRi), looking for ECM binding partners. Both PDIs bind heparan sulfate; none of them binds collagens; each of them binds further ECM components, possibly linked to the different tropisms. We investigated by small-angle X-ray scattering both PDIs structures and those of a few complexes with host partners, in order to better understand the differences within this conserved family fold. Furthermore, we highlighted a previously undisclosed moonlighting behaviour of both PDIs, namely a concentration-dependent switch of function from thiol-oxidoreductase to holdase. Finally, we have tried to exploit the differences to look for possible compounds able to interfere with the redox activity of both PDI.

Vector borne diseases (including malaria, Dengue, human trypanosomiasis, leishmaniasis, schistosomiasis and Chagas disease) are major threats to human health worldwide[1]. Despite the diversity of pathogens, which range from virus to protists to worms, all of them do not induce stable immunity, therefore vaccines based on humoral response have a low protection rate, when available[2–5]. The life cycles of these parasites were defined over 100 years ago, however the strategies they use to optimize their successful transmission are only starting to be understood at the molecular level. Parasites are now known to monitor their environment in both their host and vector and in response to other parasites. This allows them to adapt their developmental cycles and to counteract any unfavourable conditions they encounter[6].

Understanding the molecular and immunological mechanisms of the crosstalk between the parasite and the host is a prerequisite for rational vaccine discovery and drug development.

Here we focus on two human co-endemic parasites, *Leishmania major* and *Schistosoma mansoni*, because before reaching their ultimate target they both contact the extracellular matrix (ECM) of the host, especially in the dermis[7,8]. *L. major*, one of the causative agents of cutaneous leishmaniasis, is an intracellular eukaryotic parasite targeting macrophages. *S. mansoni*, the widest spread agent of intestinal schistosomiasis, is a multicellular digenean extracellular trematode, capable to finely tune the inflammatory response mediated by lymphocytes and macrophages.

We have focussed our research on protein disulfide isomerases (PDI), which are moonlighting proteins, abundantly found in both parasites secretomes and are putative therapeutic/vaccine targets[9–15]. PDIs are widespread and highly conserved proteins, belonging to the large thioredoxin (Trx) superfamily, and are modular proteins

[1]Department Biochemical Sciences, Sapienza University of Rome, P.le Aldo Moro 5, Rome, 00185, Italy. [2]ICBMS UMR 5246, CNRS - Université de Lyon, 43 Boulevard du 11 Novembre 1918, Villeurbanne, cedex, 69622, France. Correspondence and requests for materials should be addressed to S.R.-B. (email: sylvie.ricard-blum@univ-lyon1.fr)

containing between 2 and 4 Trx-like domains[16,17]. They catalyse the oxidation and/or shuffling of disulphides in substrate proteins and are involved in oxidative folding, mediated by their disulphide bond of high reduction potential and a thiol group of low pKa. The active site is composed of a CXXC motif and by a cleft capable to host a variety of large peptidyl substrates[16,17]. Most of the members of the PDI family also contain the endoplasmic reticulum (ER) retention signature (K/HDEL) and a non-canonical signal peptide for export. PDIs from pathogens have recently come centre stage for their "*Janus*" behaviour[18]. Indeed these proteins can exist in two forms: a cytosolic/ER one and a tegument/extracellular one, independently of the presence of a signal peptide for secretion. They act intracellularly as oxidative chaperones, but when secreted by the parasites they interact with host proteins, possibly modulating the host response. Sometimes they are also helped by the host PDI as documented for *L. chagasi* and Dengue virus[19,20].

The human extracellular matrix (ECM) is composed of proteins, proteoglycans and glycosaminoglycans (GAGs), and plays structural and functional roles also in host-parasite interactions[7,21–25]. ECM undergoes remodelling and dynamic reorganization in both physiological and pathological conditions, including parasitic diseases[23,26–28], which trigger the release of bioactive fragments of ECM proteins, called matricryptins[29]. These last regulate diverse processes, including angiogenesis, tumor growth and growth-factor mediated signalling pathways[29,30]. Moreover, the matrycryptin endostatin binds intact *Leishmania* promastigotes, thus contributing to their interactions with the host ECM[23].

In this study we present the structure, enzymatic activity and interactions established by two parasite PDIs, namely *L. major* PDI (LmPDI) and *S. mansoni* PDI (SmERp60), with the ECM of the human host. To the best of our knowledge this is the first time these two enzymes are comparatively characterized. The structure of both proteins was determined by SAXS and their interactions with host proteins and GAG arrays were identified by surface plasmon resonance imaging (SPRi), a method we have successfully used to build the interaction repertoire between 24 strains of *Leishmania* and the human host ECM[23]. We show that both proteins are monomeric, as the two major PDIs from the human host (HsPDIA1 and HsPDIA3/HsERp57). Both LmPDI and SmERp60 are able to reduce insulin disulphide bonds and di-eosin glutathione disulphide (di-eosin-GSSG), and both display a previously undisclosed concentration-dependent switch of function from oxido-reductase to holdase. Interestingly, LmPDI has a temperature-dependent redox activity and undergoes a reversible cold denaturation, similarly to what reported for *Saccharomyces cerevisiae* PDI (ScPDI), the only other eukaryotic full length PDI structure present in the PDB[31,32]. Finally, the structure in solution of the complexes formed with interacting GAGs was also investigated by size exclusion chromatography (SEC) coupled to SAXS (SEC-SAXS).

Results

Structural features of LmPDI and SmERp60. The genes encoding LmPDI and SmERp60 were cloned, the corresponding proteins were expressed in *E. coli* and purified to homogeneity by affinity chromatography, as reported in the Methods section. Both proteins were concentrated by ultrafiltration and then either used straight away or stored at 4 °C.

The sequences of the Trx-like domains are well conserved among LmPDI, SmERp60 and the human host most abundant PDIs (HsPDIA3/ERp57, UniProtKB P30101; HsPDIA1, UniprotKB P07237) (Fig. 1a,b), but the loops connecting the four Trx-like domains are less conserved. In the alignment shown in Fig. 1a we have also included the baker's yeast PDI (ScPDI), which is the only other eukaryotic full length PDI present in the PDB (2B5E and 3BOA) and the only one reported to be temperature sensitive[31,32]. In all PDIs the two external domains (conventionally named *a* and *a*′[16,17]) contain the catalytic Cys pair and display a higher sequence identity (Fig. 1a), while the two central ones (*b* and *b*′) are catalytically inactive and more variable in the sequence, leading to an overall low sequence identity among the 4 proteins (Fig. 1b). It is worth noticing that the linker between *b* and *b*′ and the one between *b*′ and *a*′ display fewer identical residues and different lengths (Fig. 1a, sequence between β12 and β13 and between β15 and α12). The secondary structure of recombinant LmPDI and SmERp60 was analysed by circular dichroism (CD, Fig. 1c). The content of beta strands and coiled portions computed from the CD spectra was in line with that inferred from HsPDIA3/ERp57 crystal structure (PDB 3F8U[33]); however, there was a higher content of alpha helix in LmPDI with respect to SmErp60 and HsPDIA3/ERp57 (Table 1), making it more similar to the secondary structure content of the yeast homologue ScPDI (Table 1) computed from the crystal structure (PDB 2B5E[31]).

In order to get more information into the size and shape of LmPDI and SmERp60, we used SAXS both under flow in a sample changer (Fig. 2) and coupled to a HPLC size exclusion chromatography (SEC-SAXS; Supplementary Fig. S2). The SAXS data (summarised in Table 2) suggested that both proteins are monomers, with LmPDI being compact, and SmERp60 highly flexible. In fact scattering data from LmPDI were fitted with a compact elliptical particle (as shown in the Kratky plot representation in Fig. 2a), whose radius of gyration (Rg) is 3.8 nm and the maximal particle dimension (D_{max}) is 12 nm. In contrast, the scattering data of SmERp60 were compatible with a multi-domain protein carrying flexible linkers (Fig. 2b). LmPDI is as compact as the protein from baker's yeast (ScPDI) [PDB: 2B5E[31]], whose monomer can be fitted into the reconstructed LmPDI's envelope ($\chi^2 = 1.03$, Fig. 2d). Interestingly, both LmPDI and ScPDI have a temperature sensitive structure: in fact the yeast protein has been crystallized as dimer at room temperature (22 °C) and as a monomer at 4 °C (PDB 3BOA and 2B5E, respectively[31,32]). LmPDI is a compact monomer at 20 °C, while unfolded and partially aggregated at 5 °C (Supplementary Fig. S1). Therefore it undergoes a cold denaturation, with loss of function that can be rescued by heating the sample at 37 °C (see next paragraph). This refolding step is complete when the purified protein is conserved at 4 °C, while the functional rescue is very low (if any) after freeze-thaw at −20 °C.

The conformational flexibility of SmERp60 was explored by the Ensemble Optimization Method (EOM[34]), suggesting that it might adopt an ensemble of conformations (insert of Fig. 2b) with Rg ranging from 3 to 6 nm and D_{max} from 11 to 16 nm. We also used single value deconvolution to extract the 3 most representative conformations, which were interpreted by fitting the deposited crystal structures of HsPDIA3/ERp57 (2H8L,[35], 3F8U[33],) and HsPDIA1 (4EKZ, 4EL1[36],), because they shared the highest sequence identity with SmERp60 (Fig. 1a,b). The

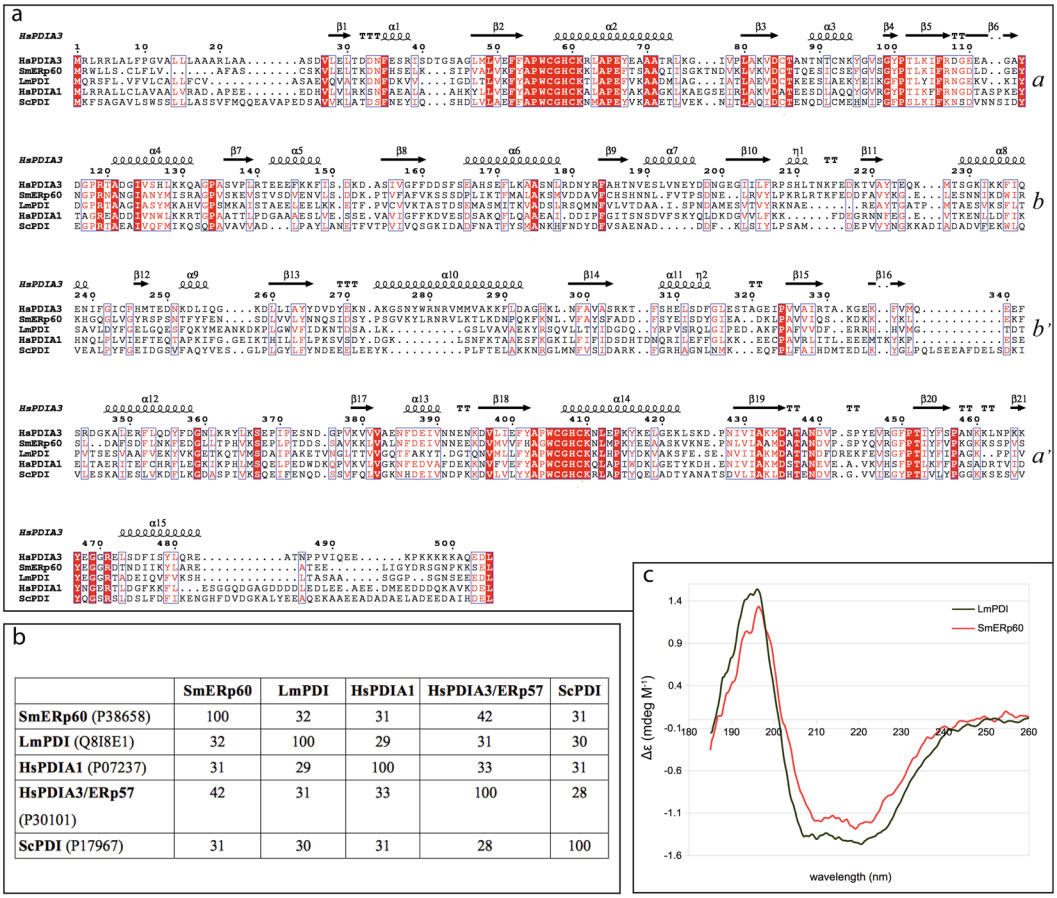

Figure 1. Primary and secondary structure comparison of *S. mansoni* and *L. major* Protein Disulfide Isomerases. Panel (**a**) Primary structure alignment of LmPDI and SmERp60 with the human host closest homologues (HsPDIA3/ERp57, HsPDIA1) and with *Saccharomyces cerevisiae* PDI (ScPDI). The alignment was performed with ClustalOmega on the EBI server[76] and rendered with ESPript 3.x[77], the secondary structure of HsPDIA3/ERp57, based on the crystallographic structure (3F8U[33]), is displayed on top of the alignment. Each line roughly represents one Trx-like domain, indicated as *a*, *b*, *b*′ and *a*′ (see text). Panel (**b**) Pairwise sequence identity matrix of human (Hs), parasites (Lm and Sm) and yeast (Sc) PDIs as computed by ClustalOmega on the EBI server[76], values are % of identical residues. The codes within the parenthesis are the UniProtKB accession numbers of each protein[78]. HsPDIA1, *Homo sapiens* PDI isoform A1; HsPDIA3/ERp57, *H. sapiens* PDI isoform A3, also known as ERp57; LmPDI, *Leishmania major* PDI; SmERp60, *Schistosoma mansoni* Endoplasmic Reticulum protein 60; ScPDI, *Saccharomyces cerevisiae* PDI. Panel (**c**) Secondary structure analysis of the recombinant proteins by circular dichroism. Spectra of SmERp60 (red) and LmPDI (green) at 25 °C, after buffer subtraction and averaging of seven sequential acquisitions on a Jasco J-810 instrument, are presented.

	SmERp60	LmPDI	HsPDIA3/ERp57	ScPDI
α helix	28	41	*32*	*38*
β-strand	26	18	*21*	*19*
β-turn	17	12	*15*	*12*
unstructured (including random coil)	28	26	*32*	*30*

Table 1. Secondary structure content (%) calculated from deconvolved CD spectra performed on the DichroWeb server[65], using CDSST3 and SELCON3 with sp175 set[66]. For comparison, secondary structures of host HsPDIA3/ERp57 and yeast ScPDI derived from the respective crystal structures (PDB 3F8U[33] and 2B5E[31]) using DSSP on the 2Struc database[79] are also reported in italics.

results suggested a butterfly movement of the external *a* and *a*′ catalytic domains with respect to the central fixed *b*-*b*′ domains, from a close to an open conformation (Fig. 2e left to right). The importance of such a flexibility of PDI superfamily to better adapt to diverse substrates was also recently reviewed by Freedman and co-workers[17].

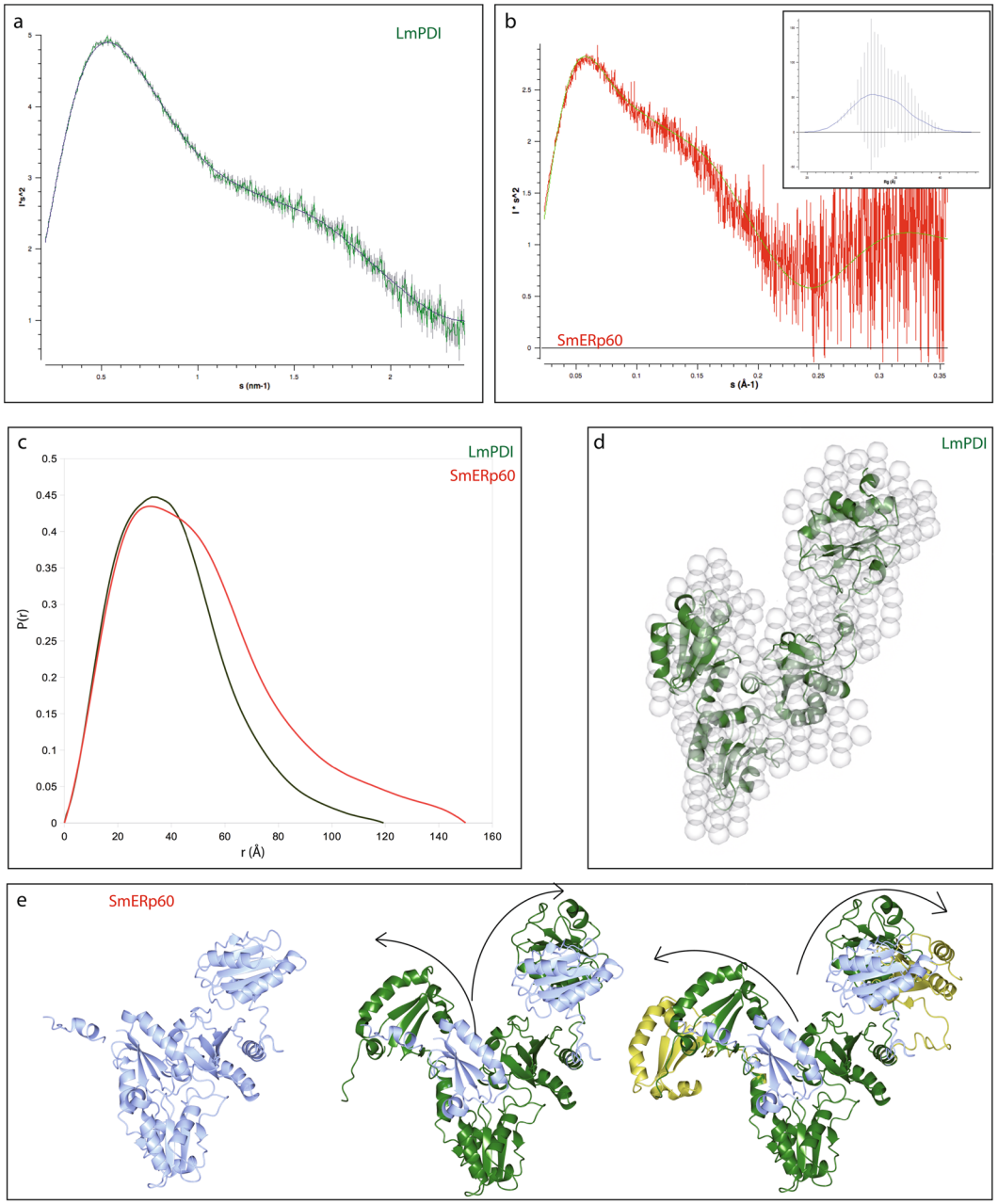

Figure 2. SAXS analysis of LmPDI and SmERp60 size and shape. Panel (a) Kratky plot of LmPDI (green) scattering curve, fitted with GNOM on the ATSAS suite[69]. Panel (b) Kratky plot of SmERp60 (red) scattering curve, fitted with the combination of conformations found after the deconvolution analysis. In the insert is shown the distribution of Rg of the particles, as computed by EOM[34]. Panel (c) Superposition of the pair probability distribution functions of SmERp60 (red) and LmPDI (green), as computed with the ATSAS suite[69]. Panel (d) *Ab initio* SAXS envelope of LmPDI, calculated by DAMIN/DAMMIF[72,73], with the yeast ScPDI structure (2B5E) docked with Supcomb, all programs were run from the ATSAS suite[69]. Panel (e) Superimposed models of the 3 possible conformations of SmERp60 (blue, green and gold) compatible with SAXS data fitting after EOM[34]. The crystal structures of HsERp57/PDIA3 (3F8U[33]) and HsPDIA1 (4EL1 and 4EKZ[36]) have been used as template models to fit the deconvolved SAXS spectra. 3D images were produced with CCP4MG[75].

Disulfide reductase and chaperone activity of LmPDI and SmERp60. The ability of both recombinant proteins to reduce disulfide bonds was assayed using the classic turbidity test, based on the precipitation of reduced insulin chains[37] (Fig. 3a,b) and also measured by fluorescence spectroscopy using di-eosin oxidised glutathione (di-eosin-GSSG) as substrate (Supplementary Fig. S5). The rate of reduction was 11.6 s^{-1} for SmERp60 and 24.3 s^{-1} for LmPDI, values in the same range of the human enzyme (16.8 s^{-1} for HsPDIA3/ERp57).

In the turbidity test, both freshly prepared SmERp60 and LmPDI were active at the concentrations tested (20–500 nM). At 20 °C and 37 °C SmERp60 had a lag time of 150 s and a rate constant of 0.46 ΔA_{600} min^{-1}; the

	LmPDI	SmERp60
Concentration range (mg ml^{-1})	0.5–6	0.5–5
Temperature (K)	293	293
Structural parameters		
Rg (nm) [from P(r)]	3.5 ± 0.3	3.98 ± 0.1
Rg (nm) [from Guinier]	3.2 ± 0.2	3.88 ± 0.1
D_{max} (nm)	11.0 ± 1	13.91 ± 0.5
Porod volume estimate (nm^3)	95 ± 15	92 ± 25
Dammif excluded volume (nm^3)	140 ± 15	141 ± 18
Molecular mass determination		
Molecular mass (kDa) [from Porod invariant][69]	56 ± 15	76 ± 15
Molecular mass (kDa) [from SAXSMoW website][80]	58	77
Theoretical molecular mass (kDa) [from ProtParam][81]	51.8	54.5

Table 2. Summary of SAXS analysis on the recombinant untagged parasite proteins LmPDI and SmERp60 collected at BM29[68] with the automatic sample changer, under continuous flow. The buffer (50 mM Tris/HCl, 150 mM NaCl, pH 7.4) was recirculated before and after every sample. Exposure time 1 s, beam attenuation (to avoid radiation damage) 50%. Ten images per each concentration were collected and averaged. The Molecular mass was derived thanks to the calibration with a BSA stock solution.

reaction was both temperature- and concentration- independent. On the other hand, LmPDI redox activity was indeed concentration-independent, but the slope at 20 °C was 0.22 ΔA_{600} min^{-1}, with a lag time of 450 s, while at 37 °C the slope was 0.67 ΔA_{600} min^{-1}, with a lag time of 90 s. As a control, *S. mansoni* Trx (SmTrx) at 20 °C and 100 nM was able to start the reaction after 100 s with a slope of 0.35 ΔA_{600} min^{-1}, as previously reported[38].

However, LmPDI was inactivated after one cycle of freeze-thawing, but it was able to regain activity when stored at 4 °C and incubated at 37 °C, prior to the experiment. In contrast, SmERp60 remained enzymatically active for 3 weeks at 4 °C and after three freeze-thaw cycles, unfortunately its inactivation was irreversible.

The purification in high yield of both parasite proteins highlighted a behaviour previously not reported. The insulin reduction assay is usually performed with PDI concentrations ranging between 10 and 100 nM, independently if the proteins are recombinant or native. In our work, we managed to raise the concentration in the assay up to 500 nM for both proteins and to 1 μM for SmERp60. Starting from 120–200 nM neither LmPDI nor SmERp60 were able to fully precipitate the insulin, always present in the assay in large excess (Fig. 3a,b). The prevention of precipitation of misfolded proteins is a feature shared by the holdases, ATP-independent chaperones, which are able to keep in quarantine misfolded proteins, avoiding aggregation[39]. A role of PDIs in the oxidative folding/refolding has already been reported in the literature [see[16,17,40,41] for reviews], but a concentration dependent switch of function, from redox to chaperone, is a novelty. It is worth to note that PDIs are abundant in the parasites secretomes, therefore we may speculate that such a switch of function may play a role in the infection. Moreover we found that bacitracin, a widely used inhibitor of PDIs, with a controversial mechanism of action[42], was able to inhibit the holdase function and to restore the oxidative power of both SmERp60 and LmPDI (Supplementary Fig. S6). In fact, when bacitracin (0.5 to 2 mM) was incubated with 500 nM SmERp60 and LmPDI, the precipitation of insulin started with a shorter lag time (more evident in SmERp60 than LmPDI) and the total absorbance went back to about 75–80% of the values obtained when the PDIs were used at lower concentrations (20–100 nM) (Fig. 3a,b *vs* Fig. S6).

Given that in *Caenorabditis elegans* and in *Dirofilaria immitis*, respectively a non parasitic and a parasitic worm, PDIs were reported to have a transglutaminase (TGase) activity[43,44], we checked for this possibility, but no TGase activity was detected on either proteins, using a commercial colorimetric assay (TG2-CovTest, Covalab, Villeurbanne, France).

Identification of binding partners of LmPDI and SmERp60 by SPR imaging. LmPDI and SmERp60 were circulated over gold affinity chips on which 76 ECM components and secreted macromolecules were spotted (the entire list is given in Supplementary Table S1). The identified partners of both PDIs are shown in Table 3. None of parasites PDI bound to proteoglycans or to collagens I to VI (neither native nor denatured), fibronectin, laminin-111, ECM-1 protein, thrombospondin-1, and vitronectin. In contrast, both proteins bound to heparan sulfate (HS). LmPDI bound also hyaluronan (HA) and SmERp60 interacted with tropoelastin, plasminogen, the GAG chondroitin sulfate (CS), and the ectodomain of the tumor endothelial marker 8 (TEM-8), also known as anthrax receptor 1. To further investigate the complex formed by SmERp60 and HS, we have performed SEC-SAXS on SmERp60 alone and in the presence of HS. Indeed a shift of the elution peak of the complex towards molecular mass compatible with a 1:1 stoichiometry was measured; the envelope derived from the corresponding scattering curve (Supplementary Fig. S3) was modelled with Gasbor on the ATSAS online server (https://www.embl-hamburg.de/biosaxs/atsas-online/gasbor.php). The structure of HsPDIA3/ERp57 was docked into the envelope leaving enough density for the GAG to be modelled inside (Supplementary Fig. S3). The same procedure was repeated with LmPDI in complex with HS and HA (Supplementary Fig. S2), here as well a shift in the elution peak was assigned to the complex formation in a *bona fide* 1:1 stoichiometry. It is interesting to note the change in the Kratky plot of the extrapolated scattering curves of the LmPDI-GAG complexes with respect

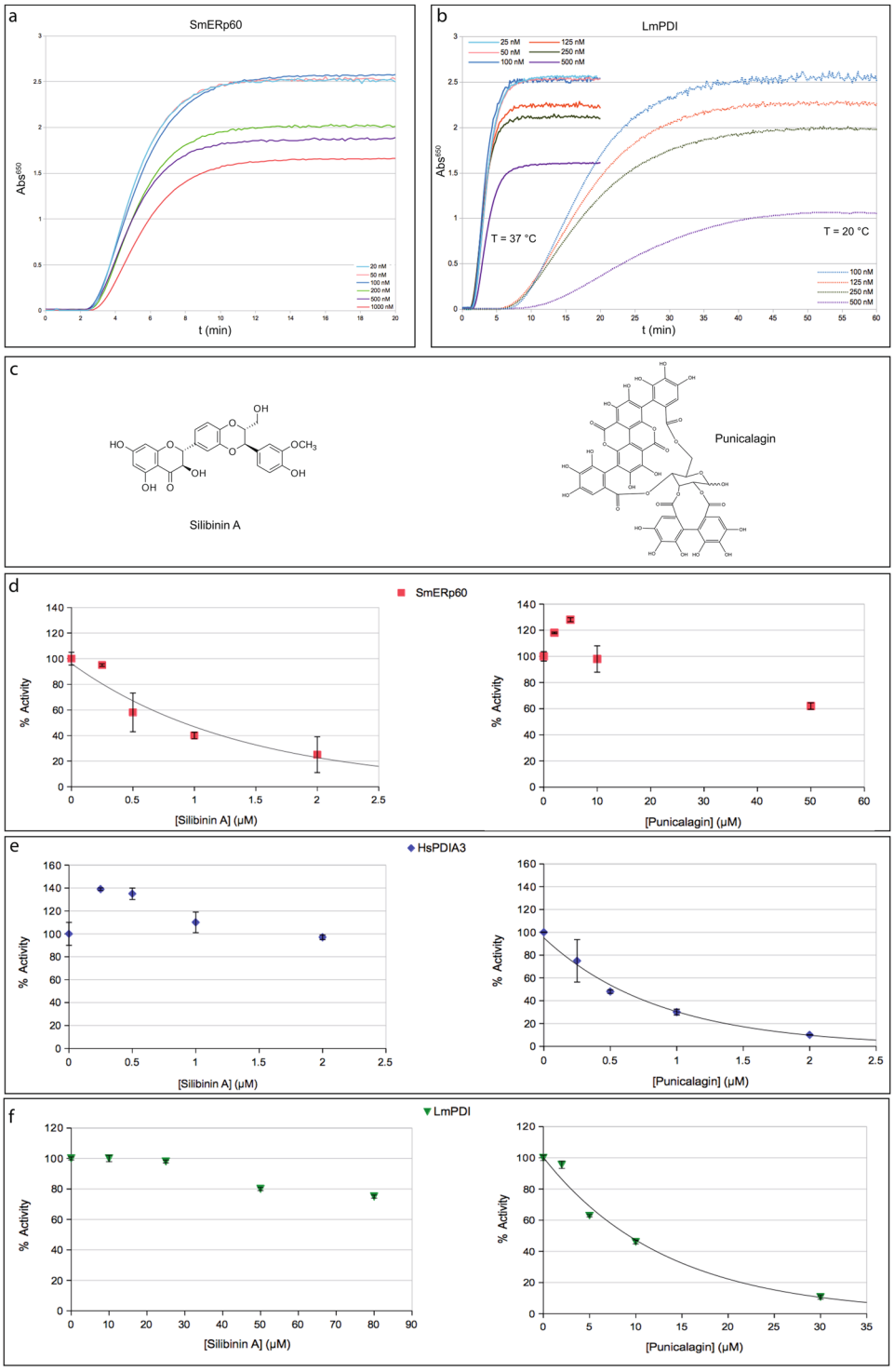

Figure 3. Redox activity of the recombinant PDIs and effect of selected natural products. Panel (a) Redox activity of SmERp60 measured at 37 °C with the turbidimetric assay. The reaction mixture contained SmERp60 at different concentrations (20, 50, 100, 200, 500 nM and 1 μM) and 130 μM insulin. The precipitation of insulin after S-S reduction was followed at 650 nm in a Cary 60 spectrophotometer (Agilent), see methods for details on the protocol. Panel (b) Redox activity of LmPDI measured with the turbidimetric assay. The assay mixture contained LmPDI at different concentrations (25, 50, 100, 125, 250 and 500 nM), 130 μM insulin. The precipitation of insulin after S-S reduction was followed at 650 nm and at two temperatures, 20 and 37 °C. Panel (c) Chemical structures of silibinin A (left) and punicalagin (right). Panel (d) Effect of selected natural products on the reduction of di-eosin oxidised glutathione by SmERp60, LmPDI and the host HsPDIA3/ERp57, followed by fluorimetry. The data are the average of 4 measurements. Redox activity of SmERp60 (50 nM), expressed as a % of reduction of di-eosinGSSG, in the presence of increasing concentrations of silibinin A (left, 0–2 μM) and punicalagin (right, 0–50 μM). Panel (e) Redox activity of host HsPDIA3/ERp57 (50 nM), expressed as a

% of reduction of di-eosinGSSG, in the presence of increasing concentrations of silibinin A (left, 0–2 μM) and punicalagin (right, 0–2 μM). Panel (f) Redox activity of LmPDI (50 nM), expressed as a % of reduction of di-eosinGSSG, in the presence of increasing concentrations of silibinin A (left, 0–80 μM) and punicalagin (right, 0– 30 μM).

to the one of LmPDI alone: there is a shift from a compact globular form to a folded, but more elongated particle, due to the elongated shape of the GAGs (Supplementary Fig. S4).

Natural compounds screening. Given the very limited number of effective drugs against schistosomiasis and leishmaniasis, and given that LmPDIs and SmErp60 are drug and/or vaccine targets[4,11], we took the opportunity to screen a subset of a natural compounds library composed by antioxidant flavonoids, already used to search for inhibitors of HsPDIA3/ERp57[45–47], which is over expressed in several cancers and is a drug target[48,49]. The rationale was to find reversible ligands, possibly able to discriminate between the host and the parasite PDIs. Among the compounds able to bind HsPDIA3/ERp57, two tannin derivatives attracted our attention: silibinin A and punicalagin (Fig. 3c). The first one is able to inhibit the redox activity of SmERp60 (IC_{50} = 750 nM), but not that of HsPDIA3/ERp57, nor of LmPDI; the second showed the exact opposite behaviour (Figs 3d *vs* 3e,f). Interestingly, silibinin A was previously reported to bind the catalytic *a/a′* domains of HsPDIA3 with a Kd = 300 nM and to enhance the internalization of the protein-silibinin A complex in HeLa cells, thus affecting the non-redox functions of HsPDIA3/ERp57[46]. Moreover, silibinin A has been reported to have anti-angiogenic properties by targeting endothelial cells in the tumor microenvironment[50]. Punicalagin inhibits both HsPDIA3/ERp57 and LmPDI, but the structural differences result in dramatically different IC_{50}, which is 0.5 μM for the host HsPDIA3/ERp57 and 7.3 μM for LmPDI. Therefore, while Silibinin A might be a good starting point to design selective anti-helminthic drugs, punicalagin might only be used in cases when the host PDI is deregulated, not when the host is infected by *Leishmania*.

Discussion

Leishmania major is one of the causative agents of cutaneous leishmaniasis; it is an intracellular eukaryotic parasite targeting macrophages of the dermal tissues. *Schistosoma mansoni* is the widest spread agent of intestinal schistosomiasis; it is a blood feeder extracellular trematode, colonizing the mesenteric veins around the liver. PDIs are widespread and highly conserved proteins mainly dedicated to oxidative folding and signalling. Despite architectural conservation, the differences in PDI's sequences might result in significant changes in dynamics and protein-protein interactions. This is especially true for the two proteins examined in this work and chosen because of their abundance in the secretomes of *L. major* and *S. mansoni*. In fact, as can be appreciated from the sequence alignment, the catalytically active Trx-like domains are well conserved among the PDIs from *H. sapiens* and both parasites, but the central redox-inactive Trx-like domains are less conserved (Fig. 1a). Moreover, the connections between the four domains differ in length between SmERp60 and LmPDI. This results in the latter assuming a compact structure, more reminiscent of the yeast PDI, as proved by SAXS, and SmERp60 being a flexible monomer, with at least three main conformations, deconvolved from SAXS data, similarly to the host homologues HsPDIA3/ERp57 (PDB 3F8U[33]) and HsPDIA1 (PDB 4EKZ, 4ELI[36]) [see also[17] for a review].

Recombinant SmERp60 is more stable than LmPDI to freeze-thaw cycles and does not display a temperature-driven function nor inactivation. This might reflect the fact that Schistosomes are adapted to environments with different temperatures: a mammalian host, a freshwater snail and freshwaters of tropical rivers/lakes.

Both recombinant PDIs show a previously undisclosed concentration-dependent switch of function from redox enzymes to holdase chaperones, indeed an example of moonlighting behaviour. Another secreted protein from *S. mansoni* showed this same behaviour, the thioredoxin peroxidase, SmPrxI, which looses its redox activity and acquires a holdase one at high concentration[51]. It will be interesting to enlarge the study to other redox proteins secreted by the parasite.

The screening of natural compounds has highlighted silibinin A as putative lead compound able to inhibit SmERp60, but not the host counterpart. It will be interesting to investigate its role *in vivo* in animal models of infection. It is worth reminding that PDIs are both intracellular and secreted proteins, so putative inhibitors might be useful in two stages of the infection. A compound targeting intracellular PDIs might interfere with its redox balance (thiol/disulfide) and therefore increase the oxidative stress in the parasites. A compound targeting secreted PDIs might interfere with host-parasite interactions and possibly limit infection.

GAGs are binding partners of both parasite PDIs (Table 3), but their repertoire is different: LmPDI binds heparan sulfate (HS) and hyaluronan (HA), while SmERp60 binds HS and chondroitin sulfate (CS). HS is known to regulate inflammation[52,53]; HA is involved in macrophage recruitment in inflammation sites[54]. In addition HS and CS have immune-modulatory properties[55,56]. The interactions of GAGs with both PDI may facilitate their attachment to the host ECM and hence host invasion. It is known that GAGs displayed at the surface of macrophages are involved in *Leishmania* recognition and uptake[7,22], we have shown by SPRi that LmPDI is one of the molecular interactors.

Schistosomes are blood feeders and live in the blood stream of the mesenteric veins, so it is not a surprise that SmERp60 binds human circulating plasminogen. At present only the secreted enolase from *S. japonicum* has been shown to bind human plasminogen[57]. SmERp60 also interacts with tropoelastin, in line with the fact that schistosomes are able to degrade elastin[58]. Interestingly, the protein interacts with Tumor Endothelial Marker 8 (TEM-8). This type I transmembrane receptor is known to be over-expressed in inflammatory processes and in cancer[59]; it is one of the receptors for the *Bacillus anthracis* protective antigen toxin and the Seneca Valley Virus[60,61]; it has

	Binding partners of SmERp60	Binding partners of LmPDI
Glycosaminoglycans		
Chondroitin Sulfate (CS)	YES	no
Heparan Sulfate (HS)	YES	YES
Hyaluronan (HA)	no	YES
Secreted proteins		
Plasminogen	YES	no
ECM proteins		
Tropoelastin	YES	no
Membrane receptors		
Tumor endothelial marker 8 (TEM8)	YES	no

Table 3. Interactions of human ECM components with recombinant purified LmPDI and SmERp60. The binding was confirmed in two independent SPRi experiments for each protein; each ECM component was spotted 3 times on each chip (see methods and supplementary material).

also been shown to modulate lymphocyte maturation and ECM remodelling[62,63]. Thus, the interaction between SmERp60 and TEM-8 suggests either a role for this receptor in host-pathogen interaction or a doorway for the parasite to hijack the host immune system. Despite LmPDI does not bind TEM-8, intact live promastigotes of *L. major* were reported to strongly interact with it[23], therefore the *Leishmania* ligand needs to be identified among other components of the secretome. Very intriguingly, while this manuscript was under revision, an *in silico* study on host-parasite interactions predicted SmERp60 to be one of the main hubs for *S. mansoni*[14], unfortunately there were no data on *L. major*, but based on our results and on our previous study on whole promastigotes[23], we may infer that LmPDI would be a player in host-parasite interactions as well.

In conclusion, LmPDI and SmERp60 are both monomeric and present a concentration-dependent switch of function from thiol-disulfide redox activity to holdase. They interact with GAGs known to regulate infection and immunity, thus these interactions may play a role in the host-parasite cross-talk. Finally, SmERp60 binds to TEM-8, which stimulates angiogenesis and serves as receptor for other pathogens; the role of this interaction in *S. mansoni* infection opens the way to further investigations.

Methods Section

Cloning expression and purification of *Leishmania major* Protein Disulfide Isomerase (LmPDI). The gene encoding for LmPDI (Q8I8E1, unreviewed entry of UniProtKB) was cloned into pET30-a vector (Novagen) within the restriction sites *BamHI* and *Eco*RI, with a sequence coding for 6His-cleavable with enterokinase (FLAG) tag at the N-terminus, using standard molecular biology techniques[64] and the primers listed in Supplementary Table S2. The vector was transformed into *E. coli* BL21(DE3) (New England Biolabs). Bacteria were grown at 37 °C in liquid LB medium (DIFCO) containing kanamycin (50 μg/ml, SIGMA) shaking at 180 rpm until Abs_{600} reached 0.6. The expression of the protein was induced overnight at 25 °C with 0.1 mM isopropyl-β-D-thio-galactopyranoside (IPTG, SIGMA). Bacteria were centrifuged 10 min at 5000 × *g* and the pellets frozen at −20 °C until use. The thawed pellets were resuspended in 50 mM Tris/HCl pH 7.4, 150 mM NaCl (TBS); then 3 U of DNase (SIGMA) and one tablet of protease inhibitors (Complete EDTA-free, Roche) was added to the resuspended pellets and incubated for 20 min on ice, before lysing the membranes by ultrasonication (Branson). Five to ten cycles of ultrasound at 40% amplitude with 5 seconds on and 10 s off pulses on ice were used to disrupt the cells. The lysed cells were then centrifuged at 4 °C for 50 min at 15000 × *g*. The supernatant was collected and the recombinant protein was purified by affinity chromatography on a Nickel-bound nitrilo-triacetic acid (Ni-NTA) agarose resin (Qiagen), equilibrated at 4 °C in TBS. The supernatant was loaded twice on the column, which was washed with 1 column volume of TBS containing 20 mM imidazole and then elution was performed with a gradient of imidazole from 20 to 500 mM in TBS. The protein eluted when the concentration of imidazole was around 200 mM and the imidazole was eliminated by dialysis in TBS, prior to protein concentration. The purity of the protein was checked by SDS-PAGE (Supplementary Fig. S7), its identity by Western Blot (mouse monoclonal Anti-Flag Ab, F3165 SIGMA) and the protein was concentrated by ultrafiltration (Vivaspin 10-kDa cutoff, Sartorius) up to 2 mg/ml and stored at 4 °C until use. The His-FLAG tag was cleaved by incubation with enterokinase (11351311001, Roche) 4 h at 20 °C and the cleaved protein was purified with an inverse affinity chromatography on Ni-NTA-agarose resin (Supplementary Fig. S7).

Cloning expression and purification of *Schistosoma mansoni* Protein disulfide isomerase (SmERp60). The sequence coding for SmERp60 (UniProtKB P38658) was cloned into pGEX4T-1 (GE-Healthcare) within the restriction sites *Bam*HI and *Xho*I, after the thrombin recognition site, using standard molecular biology techniques[64]. The plasmid was inserted into *E. coli* DH5α competent cells (New England Biolabs) by thermal shock. The transformed cells were grown in LB medium containing 100 μg/ml ampicillin (SIGMA) at 37 °C shaking at 180 rpm until A_{600} reached 0.8. Expression was then induced with 0.1 mM IPTG at 20 °C overnight. Cells were harvested by centrifuge for 10 min at 5000 × *g* and resuspended into TBS. In order to purify the recombinant protein, the cells, after the addition of 3 U DNase (SIGMA) and 1 tablet of protease inhibitor (Complete EDTA-free, Roche), were disrupted by ultrasound (on ice with 5 s pluses on and 10 s off, 40%

amplitude on a Branson instrument) and centrifuged 1 h at 15000 × *g* and 4 °C. The resulting supernatant was applied to glutathione-sepharose beads (GE-Healthcare), previously equilibrated with TBS buffer, and recirculated three times. The beads were then washed with 40 volumes of TBS and bovine thrombin [SIGMA, T4648] was added to the slurry overnight in order to cleave the GST tag. The eluate was collected, passed onto a benzamidine column (equilibrated in TBS) to remove the thrombin and concentrated up to 8 mg/ml by ultrafiltration (Vivaspin 10 kDa cutoff, Sartorius). The protein purity was assessed by SDS-PAGE (Supplementary Fig. S7).

Circular dichroism. Both purified proteins were dialysed *vs* 10 mM potassium phosphate buffer pH 7.0 before collecting seven CD spectra for each protein between 185 and 280 nm at 20 °C on a Jasco J-810 instrument. The averaged spectra, after buffer subtraction, were deconvolved and analysed on the DichroWeb website[65]. The self-consistent method for analyzing protein CD spectra, SELCON3, and CD secondary structure programme, CDSSTR[66], were used to estimate the percentage of secondary structure of recombinant PDIs (Table 1), by using the reference dataset sp175.

Identification of PDI interacting macromolecules by SPRi. SPR binding assays were performed in a Biacore Flexchip system (GE Healthcare, Facility of UMS 3444/US8, Lyon, France). Proteins (50–200 μg/ml) and GAGs (0.5–1 mg/ml) were spotted directly in triplicate onto the gold surface of a Gold Affinity chip (GE Healthcare) using a non-contact PiezoArray spotter (Perkin-Elmer Life Sciences) as previously described[23,67]. The spotted chip comprised 76 biomolecules and controls (buffers and tags) (see Supplementary Table S1 for a complete list). The chip was blocked with a buffer containing mammalian proteins (Flexchip blocking buffer, GE Healthcare) for 5 times for 5 minutes each. The blocked chip was then equilibrated with 10 mM Hepes pH 7.4, 150 mM NaCl, 0.05% Tween 20 (HBS-T) at 500 μl/min for 90 min. LmPDI and SmERp60 were diluted in HBS-T at a final concentration of 500 nM and injected over the chip surface at 25 °C for 25 min at the same flow rate. The dissociation of the complexes was monitored in HBS-T flow for 40 min. Data collected from reference spots (gold surface) and from buffer spots were subtracted from those collected on spotted proteins or GAGs to obtain specific binding curves. The binding was confirmed in two independent SPRi experiments for each recombinant protein. Since each biomolecule was spotted in triplicate on each chip, the results were the average of six sensorgrams; any given interaction positive for >4/6 was considered true.

Disulfide reductase activity assays. The capability of SmERp60 and LmPDI to reduce disulfide bonds was assessed by two methods: a standard turbidimetric assay using insulin as a substrate[37]; and a fluorimetric assay using oxidised glutathione conjugated with eosin (di-eosin-GSSG[45]).

Insulin (I6634, SIGMA) was dissolved in 20 mM Tris/HCl buffer pH 8. The solution was then acidified to pH 2–3 and quickly titrated back to pH 8. This procedure leads to the cleavage of the polypeptide into two chains, linked by a disulphide bond. The reduction of this disulphide bridge causes the separation of the two insulin chains and their precipitation, with consequent increase in the turbidity of the solution that can be monitored by measuring the absorbance at 650 nm on a Cary 60 spectrophotometer (Agilent). The assay mixture contained 0.1 M potassium phosphate buffer pH 7.0, 1 mM EDTA, 130 μM insulin, 500 μM dithiothreitol (DTT) and varying concentrations of SmERp60 and LmPDI ranging from 20 to 500 nM. A control reaction was performed by omitting the enzyme. All the assays were performed at 25 °C and at 37 °C. *S. mansoni* thioredoxin (SmTrx) was used as a positive enzyme control[38].

The fluorescent probe di-eosin-GSSG ($\lambda_{exc} = 520$ nm; $\lambda_{em} = 545$ nm) was used as alternative to turbidimetry to check the reduction of disulphide bridges. To produce the probe, 1 ml of GSSG (SIGMA) 0.1 mM was incubated with 1 mM eosin-5-isothiocyanate (SIGMA) in 100 mM potassium phosphate, 0.2 mM EDTA pH 8.8, for 1 h at room temperature. The reaction mixture was purified on a G-25 column equilibrated with 100 mM potassium phosphate, 0.2 mM EDTA pH 7.0. The elution was monitored by measuring the absorbance at 525 nm and the concentration of di-eosin-GSSG was calculated by using the extinction coefficient $\varepsilon_{525} = 88000\ M^{-1}cm^{-1}$. The assay mixture contained 50 nM protein (HsERp57/PDIA3, SmERp60, LmPDI), 200 nM di-eosin-GSSG, 5 μM DTT in PBS 1X, 0.2 mM EDTA pH 7.4. For the inhibition studies, increasing concentrations (0.2–50 μM) of punicalagin and silibinin A (Sapienza collection of natural compounds, Sapienza University of Rome, Italy) were added to the above reaction mixture and the fluorescence quenching was monitored at 545 nm ($\lambda_{exc} = 520$ nm) on a Jasco FP8500 spectrofluorimeter.

Structural analysis by Small Angle X-ray Scattering (SAXS). Data collection for the SAXS studies was initially performed at the BioSAXS beamline P12 of PETRAIII (Hamburg, Germany) using serial dilutions of SmERp60 from 6 to 0.5 mg/ml and of LmPDI from 2 to 0.5 mg/ml. Further analysis on new batches of purification was then performed at BioSAXS beamline BM29 of ESRF (Grenoble, France)[68], where the wavelength was 0.9998 Å and the sample to detector distance 2.8 m. Size exclusion chromatography was performed on a HPLC system (Shimadzu) in line with BM29 beamline (SEC-SAXS). Several samples concentrated from 4 to 10 mg/ml were automatically injected (50 μl) into a Superdex S200 5/150 (GE Healthcare), previously equilibrated with TBS. The column was run at 20 °C with a constant flow of 0.2 ml/min and 1 image/s was collected. The scattering images were collected on a Pilatus 1 M detector (Dectris) and converted into 1d profiles with BsXCube; the scattering profiles were analysed off-line using the suite ATSAS[69]. Scattering of the buffer was subtracted as background from the protein measurements with PRIMUS. HPLC-SAXS data were analysed with CHROMIXS[70] and US-SOMO[71]. The evaluation of the radius of gyration (Rg) and the forward scattering intensity (I(0)) were performed using the Guinier approximation. *Ab initio* analysis was performed either locally with DAMMIF/DAMMIN[72] or online with GASBOR (https://www.embl-hamburg.de/biosaxs/atsas-online/gasbor.php); validation and averaging was performed with DAMAVER[73]; rigid body modelling of known structures into SAXS

envelope was performed with SUPCOMB[69]. Flexibility was checked with EOM using the default parameters (10000 initial native-like models and constant subtraction allowed)[34]; the final selection retained 3 final structures, built starting from the *a*, *a′*, *b*-*b′* modules of HsPDIA3/ERp57 and HsPDIA1. The model intensities were back computed with CRYSOL[74] and 3D graphics were produced with CCP4MG[75].

References

1. World Health Organization (WHO). Integrating neglected tropical diseases into global health and development: fourth WHO report on neglected tropical diseases. WHO Report Series, Geneve. ISBN: 978924156544 8 (2017).
2. Molehin, A. J. *et al*. Cross-species prophylactic efficacy of Sm-p80-based vaccine and intracellular localization of Sm-p80/Sm-p80 ortholog proteins during development in Schistosoma mansoni, *Schistosoma japonicum*, and *Schistosoma haematobium*. *Parasitol Res.* **116**, 3175–3188 (2017).
3. Torresi, J., Ebert, G. & Pellegrini, M. Vaccines licensed and in clinical trials for the prevention of dengue. *Hum. Vaccin Immunother.* **13**, 1059–1072 (2017).
4. Tuju, J., Kamuyu, G., Murungi, L. M. & Osier, F. H. A. Vaccine candidate discovery for the next generation of malaria vaccines. *Immunology.* **152**, 195–206 (2017).
5. Tebeje, B. M., Harvie, M., You, H., Loukas, A. & McManus, D. P. Schistosomiasis vaccines: where do we stand? *Parasit Vectors.* **9**, 528 (2016).
6. Antonovics, J. *et al*. The evolution of transmission mode. *Philos. Trans. R. Soc. Lond. B Biol. Sci.* **372**, 20160083 (2017).
7. de Menezes, J. P., Saraiva, E. M. & da Rocha-Azevedo, B. The site of the bite: *Leishmania* interaction with macrophages, neutrophils and the extracellular matrix in the dermis. *Parasit. Vectors.* **9**, 264 (2016).
8. McManus, D. P. *et al*. Schistosomiasis. *Nat. Rev. Dis. Primers.* **4**, 13 (2018).
9. Cass, C. L. *et al*. Proteomic analysis of *Schistosoma mansoni* egg secretions. *Mol. Biochem, Parasitol.* **155**, 84–93 (2007).
10. Chenik, M. *et al*. Approaches for the identification of potential excreted/secreted proteins of *Leishmania major* parasites. *Parasitology.* **132**, 493–509 (2006).
11. Ben Khalaf, N., De Muylder, G., Louzir, H., McKerrow, J. & Chenik, M. *Leishmania major* protein disulfide isomerase as a drug target: enzymatic and functional characterization. *Parasitol. Res.* **110**, 1911–1917 (2012).
12. Cao, X. *et al*. Cloning, expression and characterization of protein disulfide isomerase of *Schistosoma japonicum*. *Exp. Parasitol.* **146**, 43–51 (2014).
13. Jaiswal, A. K. *et al*. Th1 stimulatory proteins of *Leishmania donovani*: comparative cellular and protective responses of rTriose phosphate isomerase, rProtein disulfide isomerase and rElongation factor-2 in combination with rHSP70 against visceral leishmaniasis. *PLoS One.* **9**, e108556 (2014).
14. Neves, L. X., Sanson, A. L., Wilson, R. A. & Castro-Borges, W. What's in SWAP? Abundance of the principal constituents in a soluble extract of *Schistosoma mansoni* revealed by shotgun proteomics. *Parasit. Vectors.* **8**, 337 (2015).
15. Cuesta-Astroz, Y., Santos, A., Oliveira, G. & Jensen, L. J. Analysis of Predicted Host-Parasite Interactomes Reveals Commonalities and Specificities Related to Parasitic Lifestyle and Tissues Tropism. *Front. Immunol.* **10**, 212 (2019).
16. Ali Khan, H. & Mutus, B. Protein disulfide isomerase a multifunctional protein with multiple physiological roles. *Front. Chem.* **2**, 70 (2014).
17. Freedman, R. B. *et al*. 'Something in the way she moves': The functional significance of flexibility in the multiple roles of protein disulfide isomerase (PDI). *Biochim. Biophys. Acta.* **1865**, 1383–1394 (2017).
18. Parakh, S. & Atkin, J. D. Novel roles for protein disulphide isomerase in disease states: a double edged sword? *Front. Cell Dev. Biol.* **3**, e30 (2015).
19. Santos, C. X. *et al*. Protein disulfide isomerase (PDI) associates with NADPH oxidase and is required for phagocytosis of *Leishmania chagasi* promastigotes by macrophages. *J. Leukoc. Biol.* **86**, 989–98 (2009).
20. Wan, S. W. *et al*. Endothelial cell surface expression of protein disulfide isomerase activates β1 and β3 integrins and facilitates dengue virus infection. *J. Cell. Biochem.* **113**, 1681–1691 (2012).
21. Bartlett, A. H. & Park, P. W. Proteoglycans in host–pathogen interactions: molecular mechanisms and therapeutic implications. *Expert Rev. Mol. Med.* **12**, e5 (2010).
22. Merida-de-Barros, D. A., Chaves, S. P., Belmiro, C. L. R. & Wanderley, J. L. M. Leishmaniasis and glycosaminoglycans: a future therapeutic strategy? *Parasit. Vectors.* **11**, 536 (2018).
23. Fatoux-Ardore, M. *et al*. Large-scale investigation of *Leishmania* interaction networks with host extracellular matrix by surface plasmon resonance imaging. *Infect. Immun.* **82**, 594–606 (2014).
24. Jinno, A. & Park, P. W. Role of glycosaminoglycans in infectious disease. *Methods Mol. Biol.* **1229**, 567–85 (2015).
25. Aquino, R. S. & Park, P. W. Glycosaminoglycans and infection. *Front. Biosci. (Landmark Ed).* **21**, 1260–77 (2016).
26. Pino-Heiss, S., Brown, M. & McKerrow, J. H. *Schistosoma mansoni*: degradation of host extracellular matrix by eggs and miracidia. *Exp. Parasitol.* **59**, 217–21 (1985).
27. Silva-Almeida, M. *et al*. Extracellular matrix alterations in experimental *Leishmania amazonensis* infection in susceptible and resistant mice. *Vet. Res.* **43**, 10 (2012).
28. Piña-Vázquez, C., Reyes-López, M., Ortíz-Estrada, G., de la Garza, M. & Serrano-Luna, J. Host-parasite interaction: parasite-derived and -induced proteases that degrade human extracellular matrix. *J. Parasitol. Res.* **2012**, 748206 (2013).
29. Ricard-Blum, S. & Vallet, S. D. Fragments generated upon extracellular matrix remodeling: Biological regulators and potential drugs. *Matrix Biol.* **75–76**, 170–189 (2019).
30. Ricard-Blum, S. & Vallet, S. D. Matricryptins Network with Matricellular Receptors at the Surface of Endothelial and Tumor Cells. *Front. Pharmacol.* **7**, 11 (2016).
31. Tian, G., Xiang, S., Noiva, R., Lennarz, W. J. & Schindelin, H. The crystal structure of yeast protein disulfide isomerase suggests cooperativity between its active sites. *Cell.* **124**, 61–73 (2006).
32. Tian, G. *et al*. The catalytic activity of protein-disulfide isomerase requires a conformationally flexible molecule. *J. Biol. Chem.* **283**, 33630–33640 (2008).
33. Dong, G., Wearsch, P. A., Peaper, D. R., Cresswell, P. & Reinisch, K. M. Insights into MHC class I peptide loading from the structure of the tapasin-ERp57 thiol oxidoreductase heterodimer. *Immunity.* **30**, 21–32 (2009).
34. Tria, G., Mertens, H. D. T., Kachala, M. & Svergun, D. I. Advanced ensemble modelling of flexible macromolecules using X-ray solution scattering. *IUCr J.* **2**, 207–217 (2015).
35. Kozlov, G. *et al*. Crystal structure of the bb′ domains of the protein disulfide isomerase ERp57. *Structure.* **14**, 1331–1339 (2006).
36. Wang, L., Wang, X. & Wang, C.-C. Protein disulfide-isomerase, a folding catalyst and a redox-regulated chaperone. *Free Radic. Biol. Med.* **83**, 305–313 (2015).
37. Holmgren, A. Thioredoxin catalyzes the reduction of insulin disulfides by dithiothreitol and dihydrolipoamide. *J. Biol. Chem.* **254**, 9627–9632 (1979).
38. Boumis, G. *et al*. Structural and functional characterization of *Schistosoma mansoni* Thioredoxin. *Protein Sci.* **20**, 1069–1076 (2011).
39. Angelucci, F. *et al*. Typical 2-Cys peroxiredoxins in human parasites: Several physiological roles for a potential chemotherapy target. *Mol. Biochem. Parasitol.* **206**, 2–12 (2016).

40. Haque, S. J., Majumdar, T. & Barik, S. Redox-assisted protein folding systems in eukaryotic parasites. *Antioxid. Redox Signal.* **17**, 674–83 (2012).
41. Beal, D. M. *et al* Quantitative analyses of the yeast oxidative protein folding pathway *in vitro* and *in vivo*. *Antioxid. Redox Signal*. ePub ahed of print. https://doi.org/10.1089/ars.2018.7615 (2019).
42. Karala, A. R. & Ruddock, L. W. Bacitracin is not a specific inhibitor of protein disulfide isomerase. *FEBS J.* **277**, 2454–2462 (2010).
43. Eschenlauer, S. C. & Page, A. P. The *Caenorhabditis elegans* ERp60 homolog protein disulfide isomerase-3 has disulfide isomerase and transglutaminase-like cross-linking activity and is involved in the maintenance of body morphology. *J. Biol. Chem.* **278**, 4227–4237 (2009).
44. Chandrashekar, R., Tsuji, N., Morales, T., Ozols, V. & Mehta, K. An ERp60-like protein from the filarial parasite *Dirofilaria immitis* has both transglutaminase and protein disulfide isomerase activity. *Proc. Natl. Acad. Sci. USA* **95**, 531–536 (1998).
45. Trnková, L., Ricci, D., Grillo, C., Colotti, G. & Altieri, F. Green tea catechins can bind and modify ERp57/PDIA3 activity. *Biochim, Biophys, Acta.* **1830**, 2671–2682 (2013).
46. Grillo, C. *et al*. The binding of silibinin to ERp57. *Chem. Biol. Interact.* **213**, 37–43 (2014).
47. Giamogante, F. *et al*. Punicalagin, an active pomegranate component, is a new inhibitor of PDIA3 reductase activity. *Biochimie.* **147**, 122–129 (2018).
48. Hettinghouse, A., Liu, R. & Liu, C. J. Multifunctional molecule ERp57: From cancer to neurodegenerative diseases. *Pharmacol. Ther.* **181**, 34–48 (2018).
49. Gaucci, E., Altieri, F., Turano, C. & Chichiarelli, S. The protein ERp57 contributes to EGF receptor signaling and internalization in MDA-MB-468 breast cancer cells. *J. Cell. Biochem.* **114**, 2461–70 (2013).
50. Deep, G. & Agarwal, R. Targeting tumor microenvironment with silibinin: promise and potential for a translational cancer chemopreventive strategy. *Curr. Cancer Drug Targets.* **13**, 486–99 (2013).
51. Angelucci, F. *et al*. Switching between the alternative structures and functions of a 2-Cys peroxiredoxin, by site-directed mutagenesis. *J. Mol. Biol.* **425**, 4556–4568 (2013).
52. Collins, L. E. & Troeberg, L. Heparan sulfate as a regulator of inflammation and immunity. *J Leukoc. Biol.* **105**, 81–92 (2019).
53. Farrugia, B. L., Lord, M. S., Melrose, J. & Whitelock, J. M. The Role of Heparan Sulfate in Inflammation, and the Development of Biomimetics as Anti-Inflammatory Strategies. *J. Histochem Cytochem.* **66**, 321–336 (2018).
54. Petrey, A. C. & de la Motte, C. A. Hyaluronan, a crucial regulator of inflammation. *Front Immunol.* **5**, 101 (2014).
55. du Souich, P., García, A. G., Vergés, J. & Montell, E. Immunomodulatory and anti-inflammatory effects of chondroitin sulphate. *J. Cell. Mol. Med.* **13**, 1451–63 (2009).
56. Vallières, M. & du Souich, P. Modulation of inflammation by chondroitin sulfate. *Osteoarthritis Cartilage.* **18**, S1–S6 (2010).
57. Figueiredo, B. C., Da'dara, A. A., Oliveira, S. C. & Skelly, P. J. Schistosomes Enhance Plasminogen Activation: The Role of Tegumental Enolase. *PLoS Pathog.* **11**, e1005335 (2015).
58. Salter, J. P., Lim, K. C., Hansell, E., Hsieh, I. & McKerrow, J. H. Schistosome invasion of human skin and degradation of dermal elastin are mediated by a single serine protease. *J. Biol. Chem.* **275**, 38667–38673 (2000).
59. Carson-Walter, E. B. *et al*. Cell surface tumor endothelial markers are conserved in mice and humans. *Cancer Res.* **61**, 6649–6655 (2001).
60. Bradley, K. A., Mogridge, J., Mourez, M., Collier, R. J. & Young, J. A. Identification of the cellular receptor for anthrax toxin. *Nature.* **414**, 225–229 (2001).
61. Evans, D. J. *et al*. Seneca Valley Virus Exploits TEM8, a Collagen Receptor Implicated in Tumor Growth. *Front. Oncol.* **8**, 506 (2018).
62. Paccani, S. R. & Baldari, C. T. T cell targeting by anthrax toxins: two faces of the same coin. *Toxins (Basel).* 3, (660–671 (2011).
63. Besschetnova, T. Y. *et al*. Regulatory mechanisms of anthrax toxin receptor 1-dependent vascular and connective tissue homeostasis. *Matrix Biol.* **42**, 56–73 (2015).
64. Green, M. R. & Sambrook, J. Molecular Cloning: A Laboratory Manual. CSH Press ISBN: 978-1-936113-42-2 (2012).
65. Whitmore, L. & Wallace, B. A. Protein secondary structure analyses from circular dichroism spectroscopy: methods and reference databases. *Biopolymers.* **89**, 392–400 (2008).
66. Sreerama, N. & Woody, R. W. Estimation of protein secondary structure from circular dichroism spectra: comparison of CONTIN, SELCON, and CDSSTR methods with an expanded reference set. *Anal. Biochem.* **287**, 252–260 (2000).
67. Salza, R. *et al*. Extended interaction network of procollagen C-proteinase enhancer-1 in the extracellular matrix. *Biochem. J.* **457**, 137–49 (2014).
68. Pernot, P. *et al*. Upgraded ESRF BM29 beamline for SAXS on macromolecules in solution. *J. Synchrotron Radiat.* **20**, 660–664 (2013).
69. Franke, D. *et al*. ATSAS 2.8: a comprehensive data analysis suite for small-angle scattering from macromolecular solutions. *J. Appl. Crystallogr.* **50**, 1212–1225 (2017).
70. Panjkovich, A. & Svergun, D. I. CHROMIXS: automatic and interactive analysis of chromatography-coupled small-angle X-ray scattering data. *Bioinformatics.* **34**, 1944–1946 (2018).
71. Brookes, E., Vachette, P., Rocco, M. & Pérez, J. US-SOMO HPLC-SAXS module: dealing with capillary fouling and extraction of pure component patterns from poorly resolved SEC-SAXS data. *J. Appl. Crystallogr.* **49**, 1827–1841 (2016).
72. Franke, D. & Svergun, D. I. DAMMIF, a program for rapid ab-initio shape determination in small-angle scattering. *J. Appl. Crystallogr.* **42**, 342–346 (2009).
73. Volkov, V. V. & Svergun, D. I. Uniqueness of *ab-initio* shape determination in small-angle scattering. *J. Appl. Cryst.* **36**, 860–864 (2003).
74. Svergun, D. I., Barberato, C. & Koch, M. H. J. CRYSOL - a Program to Evaluate X-ray Solution Scattering of Biological Macromolecules from Atomic Coordinates. *J. Appl. Cryst.* **28**, 768–773 (1995).
75. McNicholas, S., Potterton, E., Wilson, K. S. & Noble, M. E. Presenting your structures: the CCP4mg molecular-graphics software. *Acta Crystallogr. D Biol. Crystallogr.* **67**, 386–394 (2011).
76. Sievers, F. *et al*. Fast, scalable generation of high-quality protein multiple sequence alignments using Clustal Omega. *Mol. Syst. Biol.* **7**, 539 (2011).
77. Robert, X. & Gouet, P. Deciphering key features in protein structures with the new ENDscript server. *Nucl. Acids Res.* **42**(W1), W320–W324 (2014).
78. The UniProt Consortium. UniProt: the universal protein knowledgebase. *Nucleic Acids Res.* **46**, 2699 (2018).
79. Klose, D. P., Wallace, B. A. & Janes, R. W. 2Struc: the secondary structure server. *Bioinformatics.* **26**, 2624–2625 (2010).
80. Fischer, H., Neto, deO., Napolitano, M., Polikarpov, H. B. & Craievich, I. A.F. Determination of the molecular weight of proteins in solution from a single small-angle X-ray scattering measurement on a relative scale. *J. Appl. Cryst.* **43**, 101–109 (2010).
81. Gasteiger E., *et al* Protein Identification and Analysis Tools on the ExPASy Server. (In) John M. Walker (ed.): The Proteomics Protocols Handbook, Humana Press (2005).

Acknowledgements

We thank Marie-Fatoux Ardore, who performed the preliminary trials of *L. major* PDI cloning, Francescangelo Vedele and Federica Carucci for testing the long-term storage conditions. We thank Christophe Marquette and Loïc Blum (Institut de Chimie et Biochimie Moléculaires et Supramoléculaires, UMR 5246 CNRS, Université Lyon 1, Lyon, France) and AxoScience (Villeurbanne, France) for providing access to the spotter. We are grateful

to Dr Nicole M. Thielens (Université Grenoble Alpes, IBS, UMR 5075-CNRS-CEA, Grenoble, France) for the generous gift of purified C1q, ficolin H, ficolin L and ficolin M. This work has been funded by: Sapienza University of Rome "Progetto Università no. RP116154C9527136" to AEM, University of Lyon (Programme Avenir Lyon Saint-Etienne IMPULSION 2017; and BQR 2017) to AEM; Région Rhône-Alpes, France (grant No. 1SRESR12-008697-01 SRESRI 2011 ARC No. 1) to SRB, Fondation pour la Recherche Biomédicale (grant No. DBI20141231336) to SRB; Région Auvergne-Rhône-Alpes (Grant SCUSI2018 No. P010O003) to AEM. LM was recipient of an ERASMUS + scholarship from Sapienza University of Rome. The research leading to these results was started thanks to BioStruct-X project no.1223; Giancarlo Tria from the PETRAIII P12 staff (Hamburg, Germany) is acknowledged for the collaborative project. Preliminary SEC-SAXS measurements were performed at the SWING beamline of SOLEIL (St Aubin, France) under the project 20170906. We acknowledge the European Synchrotron Radiation Facility (Grenoble, France) for provision of synchrotron radiation facilities at beamline BM29, under projects MX1920, MX1949 and MX1979.

Author Contributions

A.E.M. and S.R.B. conceived the project; S.B., L.M., B.D. cloned and produced LmPDI; A.E.M., L.M. and G.B. cloned and produced SmERp60; R.S. and S.R.B. performed SPRi and analysed the data; A.E.M., L.M., G.B., S.C. performed the functional and inhibition assays on LmPDI, SmERp60 and HsERp57/PDIA3; A.E.M. performed the SAXS experiments and analysed the data; A.E.M. and S.R.B. wrote the manuscript; all the authors read and revised the manuscript.

Additional Information

Supplementary information accompanies this paper at https://doi.org/10.1038/s41598-019-45709-8.

Competing Interests: The authors declare no competing interests.

Publisher's note: Springer Nature remains neutral with regard to jurisdictional claims in published maps and institutional affiliations.